



Temperature, pressure, and oxygen quenching behavior of fluorescence spectra and lifetimes of gas-phase *o*-xylene and 1,2,4-trimethylbenzene

Thorsten Benzler¹ · Torsten Endres¹ · Thomas Dreier¹ · Christof Schulz¹

Received: 25 October 2017 / Accepted: 27 March 2018 / Published online: 4 April 2018
© Springer-Verlag GmbH Germany, part of Springer Nature 2018

Abstract

Ortho-xylene (1,2-dimethylbenzene, XL) and 1,2,4-trimethylbenzene (TMB) are promising aromatic fluorescence tracer species for gas-phase imaging measurements of concentration, temperature, and oxygen partial pressure. In the present work, temperature-dependent gas-phase ultraviolet absorption spectra of XL and TMB were measured. In the investigated temperature range (296–725 K), the absorption bands red-shift with increasing temperature for both species and their absorption cross-sections increase. Time-resolved fluorescence spectra were recorded after picosecond laser excitation at 266 nm as a function of temperature (XL 296–1025 K, TMB 296–775 K), pressure (1–10 bar), and O₂ concentration using a streak camera coupled to a spectrometer. The fluorescence spectra of both species show a noticeable red-shift with increasing temperature and O₂ concentration. In N₂ as bath gas, the fluorescence lifetime of XL and TMB decreases by three orders of magnitude at the peak temperatures compared to room temperature. For both species, fluorescence quenching by N₂ (up to 10 bar) is temperature-dependent and is strongest at about 500 K. Quenching by O₂ shortens the fluorescence lifetime for both species significantly. This effect is much reduced at higher temperatures. The temperature dependence of the Stern–Volmer coefficients that describe the effect of O₂ quenching can be approximated by an exponential decay. Semi-empirical exponential fits to all investigated data (for XL and TMB) as well as published data for toluene were used to provide signal prediction models that are capable of predicting the signal intensities over a wide range of environmental conditions.

1 Introduction

Laser-induced fluorescence (LIF) imaging is one of the most widely applied measurement techniques for visualization of mixing processes and for determining gas-phase properties such as temperature and fuel/air ratios [1]. In these applications, tracer species with known photo-physical behavior and a high sensitivity of their fluorescence properties towards the studied parameters are added to non-fluorescent carriers (e.g., surrogate fuels and/or nitrogen or air) and the resulting signals are imaged onto cameras upon excitation of the tracers in the ultraviolet with laser light sheets. Various mixing studies have been conducted utilizing the tracer species toluene (TL), acetone, 3-pentanone, and triethylamine

(TEA) [2–4]. More recently, anisole [5] and difluorobenzene [6] have been suggested as tracers that provide particularly high signal levels [7]. In case of a liquid base fuel, it is also necessary to adjust the evaporation characteristics to the respective measurement situation and to select a tracer that does not condense at the lowest temperatures present in an experiment [1]. It has been shown that combinations of two tracers can be exploited to visualize stratification of high- and low-volatility fuel components which requires tracers that particularly well match the properties of the respective volatility class [8]. For applications in diesel engine combustion, efforts were undertaken to further extend the choice of tracer species to 1-phenyloctane and 1-phenyldecane [9] or 5-nonanone [10] that meet the higher evaporation temperatures of diesel fuel. Therefore, there is a continuous interest in obtaining the required spectroscopic data of tracer species with various molecule sizes (and thus evaporation and transport properties). The quantities of interest include absorption cross-sections and fluorescence quantum yields to enable quantitative signal evaluations in practical measurement situations as well as changes in absorption and emission

✉ Thorsten Benzler
thorsten.benzler@uni-due.de

¹ Institute for Combustion and Gas Dynamics, Reactive Fluids, University of Duisburg-Essen, Carl-Benz-Str. 199, 47057 Duisburg, Germany

spectra as a function of the bath-gas composition, temperature, and pressure.

1,2,4-Trimethylbenzene (TMB, C_9H_{12}) and 1,2-dimethylbenzene (*o*-xylene, XL, C_8H_{10}) are two of the less common aromatic tracer species employed for fluorescence diagnostics [1, 2, 11], which feature spectroscopic properties similar to the frequently applied toluene (TL), but with higher boiling points (111, 144.4, and 170 °C for TL, XL, and TMB, respectively). Due to their thermophysical properties, TMB and XL would be suitable tracers for mixing studies representing low-volatility diesel or high-volatility gasoline components. All these structural analogues, TL, as well as XL and TMB have similar fluorescence quantum yields (FQY) and are components of commercial fuels. However, since their concentrations vary and their fluorescence spectra overlap (also with additional fluorescing species), it is not possible to directly use the fluorescing components of commercial fuels for quantitative LIF measurements. Therefore, usually, non-fluorescent surrogate fuels are applied with one (or few) tracers added for visualization purposes.

For all three species, the center wavelength and spectral width of the first ($^1A_{1g} \rightarrow ^1B_{2u}$) absorption bands of interest are located in the near UV and are quite similar, because methylation does not significantly change the π -electron system [12]. For practical applications, the dependence of essential parameters governing the generated LIF signal intensity, i.e., absorption cross-sections and FQY as well as their dependence on environmental conditions, i.e., temperature, pressure, and bath-gas composition (especially oxygen content), must be known and understood before quantitative LIF measurements are feasible. Due to their dense manifolds of thermally populated vibrational energy levels in the electronic ground state, the species exhibit almost structureless absorption bands at atmospheric pressure and above [1]. Apart from the varying absorption cross-sections, varying the excitation wavelength also results in a change in excess energy in the excited state and can, therefore, influence the spectroscopic parameters [13].

Temperature-dependent relative fluorescence quantum yields for TMB have previously been determined by Rosow [14]. It was found that their variation with respect to temperature, pressure, and O_2 partial pressure is similar to that of TL. No study of the relative quantum yield of XL has been published up to now.

Fluorescence quantum yields can be derived from LIF-intensity measurements as long as the absorption cross-sections and the laser fluence are known and the tracer number densities are well controlled. Alternatively, the dependence of (relative) FQYs on environmental conditions can be determined through the measurement of effective fluorescence lifetimes [15, 16], which makes the measurement independent of the determination of the parameters mentioned above, especially the uncertainties in tracer concentrations

that often arise when preparing mixtures with bath gases at high temperatures and pressures. The fluorescence lifetime of TMB was recently presented by us for pressures up to 1 bar in the 295–475 K range [13]. We observed a change from increasing to decreasing FQY with increasing pressure for rising temperature, which could be explained by the difference of the relative thermal energy distribution and the excess energy right after excitation in the S_1 state.

The present work aims at extending the available database of XL and TMB into regimes of higher temperatures and gas pressures relevant in LIF-based optical diagnostics, e.g., in engines, shock tubes, or model gas-turbine sections. The spectral and fluorescence lifetime data are also important for the further development of existing and new photo-physical models for the prediction of FQYs of these species. In the present work, we analyze the dependence of the absorption cross-sections of TL, XL, and TMB up to 725 K and fluorescence lifetimes of XL and TMB in up to 1075 K with picosecond laser excitation at 266 nm. Because literature data on temperature- and wavelength-dependent absorption cross-sections of toluene are sparse in the practically relevant temperature region and often spectrally under-resolved (which is relevant mostly in the lower temperature and pressure regions) [17], new measurements are presented here along with the respective data for XL and TMB. Measurements were carried out in pure N_2 from 1 to 10 bar total pressure and in N_2/O_2 mixtures with varying O_2 partial pressures at 1 bar total pressure. We also compare the expected signal intensities of XL and TMB with those of TL using semi-empirical models that consider the dependence on temperature (up to 1000 K), total pressure (up to 10 bar), and oxygen partial pressure (up to 209.5 mbar).

2 Theoretical background

For single-ring aromatics, methyl substitution adds vibrational modes and, therefore, increases the vibrational state density from TL (one methyl group) via XL (two) to TMB (three). Methyl substitution also results in an increase of the absorption cross-section and a red-shift of the spectra for $S_1 \rightarrow S_0$ transitions. This is due to the decrease of the 0–0 transition energy between the ground and the excited states with an increasing number of methyl groups [12]. In addition, at a given temperature, the higher density of states leads to a shift of the mean vibrational energy towards higher levels due to the Boltzmann distribution. Because this vibrational distribution is transcribed from the ground state to the electronically excited state during laser excitation, the excess energy in the excited state for the molecules with a high density of states is even higher (and higher than a simple 0–0 transition energy consideration would suggest).

As with most single-ring aromatic hydrocarbons, the S_1 state after 266-nm excitation can undergo radiative (with fluorescence rate k_f) and non-radiative deactivation, whereby the latter processes are dominated by intersystem crossing (rate: k_{ISC}) and internal conversion (from S_1 to S_0 , rate: k_{IC}) [1]. Other collision-induced non-radiative deactivation processes k_q are electronic quenching by bath-gas molecules, including ground-state target species such as the carrier gas (e.g., N_2) and O_2 , the latter being the most efficient quencher because of its triplet ground state [1]. The total depopulation rate, k_{tot} , then is inversely proportional to the experimentally accessible effective fluorescence lifetime, τ_{eff} [18]:

$$k_{tot} = k_f + k_{ISC} + k_{IC} + k_q = \frac{1}{\tau_{eff}}. \quad (1)$$

The relation between τ_{eff} and the fluorescence quantum yield, ϕ_{fl} , is given by

$$\phi_{fl} = \frac{k_f}{k_{tot}} = \frac{\tau_{eff}}{\tau_f} = k_f \tau_{eff}, \quad (2)$$

with τ_f , the radiative lifetime [18]. Thus, the fluorescence quantum yield is proportional to the effective fluorescence lifetime τ_{eff} .

For quenching by O_2 , a Stern–Volmer relation

$$\frac{S_{fl}^0}{S_{fl}} = \frac{\tau_{eff}^0}{\tau_{eff}} = 1 + k_{SV} n_q \quad (3)$$

often holds, i.e., a linear dependence of the fluorescence signal intensity ratio S_{fl}^0/S_{fl} (and thus τ_{eff}) without (S_{fl}^0) and with (S_{fl}) presence of the quencher with its number density n_q (e.g., [14, 19, 20]). The respective Stern–Volmer factor, k_{SV} , can be extracted by linearly fitting the ratio of measured signal intensities (or fluorescence lifetime) for various quencher concentrations and the respective measured values without quenching (i.e., S_{fl}^0/S_{fl} or τ_{eff}^0/τ_{eff}) vs. the quencher concentration n_q .

The strong temperature dependence of the quantum yield and the fluorescence lifetime of toluene is explained by the vibrational excess energy that increases with temperature and boosts non-radiative relaxation processes (intersystem crossing and internal conversion) [14, 15]. The influence

of pressure on the quantum yield was described previously for TL and TMB for up to 1 bar which corresponds well to results for even higher pressures [13, 14, 21]. One, therefore, expects similar behavior for all three methyl-substituted single-ring aromatics investigated here.

3 Experiment

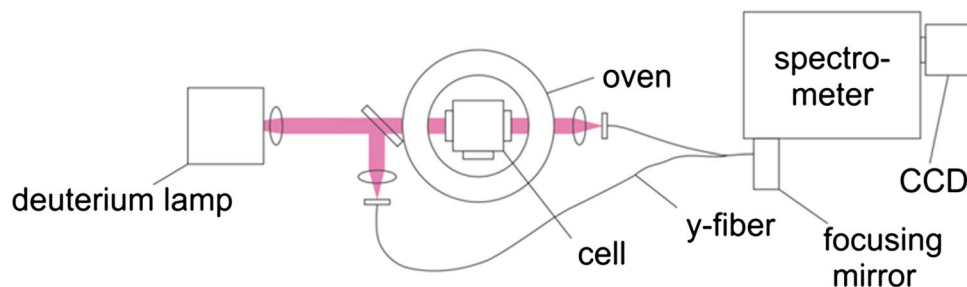
3.1 Absorption experiments

Absorption measurements were performed in an optically accessible stainless-steel high-temperature cell that is continuously purged with the respective tracer/bath-gas flow (Fig. 1) [22]. It was used at atmospheric pressure and can be heated in a cylindrical oven. The temperature was monitored by a K-type thermocouple mounted inside the cell close to the measurement volume. A deuterium lamp (LOT Oriol) was used as broadband UV light source to record absorption spectra in the 230–300 nm range. A quartz plate in front of the cell entrance window splits off part of the incoming light beam for recording I_0 . This reference signal as well as the light transmitted through the cell was then coupled into a quartz Y-fiber, spectrally dispersed by a spectrometer (Horiba, iHR320; $f=320$ mm, 1200 groves/mm grating), and detected by a CCD camera (Horiba, Syncerity; 256×1024 pixels). The Y-fiber allowed the positioning of the dispersed light from both arms on top of each other onto different regions (50×1024 pixels each) of the CCD chip—from now on referred to as “reference” and “signal”. An exposure time of 1 ms and an entrance slit of 200 μm were used to make good use of the 16 bit dynamic range of the camera while maintaining a spectral resolution of 0.47 nm (75 cm^{-1} at 250 nm). Spectra were then generated by binning over 50 rows per channel and dividing the signal by the reference.

3.2 Fluorescence experiments

The experimental setup for the time-resolved detection of fluorescence spectra is identical to the one presented in detail in Ref. [15], and therefore, only a brief description is given here. Fluorescence measurements were carried out in a gas mixture of the evaporated tracer and the respective

Fig. 1 Experimental arrangement for absorption cross-section measurements



bath gas flowing through an externally heated (up to 1200 K) cylindrical ceramic chamber contained inside an optically accessible stainless-steel pressure vessel (up to 10 bar). The tracer species were excited at 266 nm by the beam of a frequency-quadrupled picosecond Nd:YAG laser (pulse width 26 ps, at 10 Hz) with typical pulse energies of 1 mJ at the measurement volume entering and exiting through 10 mm-thick quartz windows. The signal was imaged onto the slit of a spectrograph (ARC, SP2300; $f=300$ mm, 150 grooves/mm grating) connected to a streak camera (Hamamatsu Photonics, model C5680-24C). The system thus delivers images with a wavelength (nominally 0.2 nm/pixel) and a time axis (down to 0.2 ps/pixel depending on the total duration of the time trace).

3.3 Gas handling and linearity check

TMB, XL, and TL (Merck Chemicals, for analysis grade) were filled into glass containers and bubbled through with N_2 to drive out dissolved O_2 before feeding an high-performance liquid chromatography (HPLC) pump (Bischoff-Chrom, model Compact Pump 2250). The liquids were vaporized in a heated chamber (Bronkhorst, CEM) with part of the flow of the carrier gas (vaporized from liquid N_2) and afterwards mixed with additional carrier gas. For the absorption experiment, increasing tracer concentrations (from 0.1 to 1 mbar partial pressure) were fed to the cell at each temperature to ensure that measurements took place in the linear absorption regime, which then were averaged. For the fluorescence experiments, N_2 (vaporized from liquid N_2) and compressed air were used as bath gas for pressures up to 6 bar, while gas from cylinders (Air Liquide, 4.9 grade) was used for experiments above 6 bar. To avoid condensation, all tubes were resistively heated and kept at 470 K. The O_2 partial pressure in the chamber was varied by mixing air with varying amounts of N_2 .

Fluorescence intensities were investigated as a function of laser fluence to determine the limits of the linear LIF regime (not shown here). Linear behavior was observed when the laser fluence was kept below 35 mJ/cm^2 at 296 K for XL and TMB, which is consistent with data previously reported for TL [21]. This laser fluence was used for temperatures up to 900 K. Because the saturation regime is known to shift to higher laser fluences at elevated temperatures [23], for reasons of gaining a better signal-to-noise ratio, the fluence level was increased stepwise to 50 mJ/cm^2 at the highest temperatures investigated which was also checked to be in the linear regime. The partial pressures of XL and TMB were set to 1.8 mbar at 296 K (20 $\mu\text{l/min}$ liquid tracer in 2 l/min buffer gas; number density $\sim 4 \times 10^{22} \text{ m}^{-3}$). At higher temperatures, the liquid flow of the tracer was increased to maintain a nearly constant number density in the probe volume. In additional measurements, it was tested that, at these number densities and laser fluences,

Table 1 Experimental conditions for spectral and fluorescence lifetime measurements presented in this work

	XL		TMB	
	Spectra	Lifetimes	Spectra	Lifetimes
T (K)	298–1075	298–1075	298–1025	298–1075
p_{tot} (bar)	1–10		1–10	
p_{O_2} (mbar)	5.1–210		8.7–210	

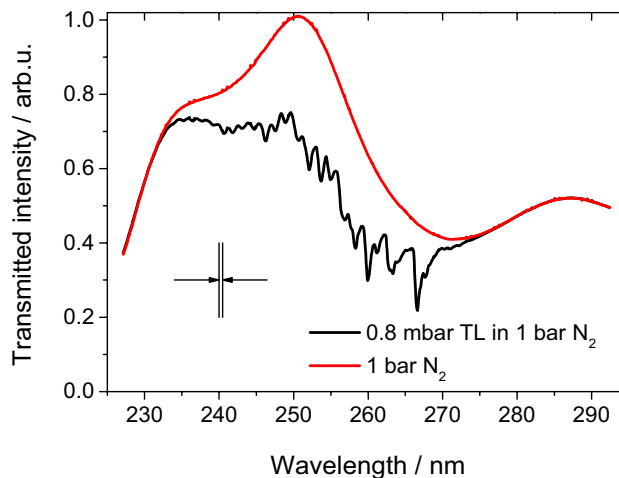


Fig. 2 Spectral intensity distribution of deuterium lamp transmitted through the N_2 -filled cell (red line) and after filling with 0.8 mbar TL in 1 bar N_2 at 296 K (black line). The arrows indicate the spectral resolution of the detection system of 0.47 nm (FWHM)

self-quenching [24] can be neglected. The temperature, pressure, and bath-gas conditions in the absorption and fluorescence experiments are summarized in Table 1.

4 Data evaluation

4.1 Absorption experiments

For each lamp-based measurement, 200 camera images with detection times of 50 ms each were averaged for noise reduction. Figure 2 shows sample spectra of the deuterium lamp intensity (signal) through the N_2 -filled cell ($I_0(\lambda)$, red line) and with a mixture of toluene (partial pressure 0.8 mbar) in 1 bar N_2 at 296 K ($I(\lambda)$, black line). After dark-signal subtraction, the absorption cross-section was then calculated using Lambert–Beer's law

$$\sigma(\lambda) = \frac{\ln\left(\frac{I_0(\lambda)}{I(\lambda)}\right)}{d n}, \quad (4)$$

with the absorption path length d as the distance between the quartz windows (11 cm), and the tracer number density

n. Both measurements, with and without tracer, were conducted for all temperatures, since the transmission characteristics of the cell slightly changed with temperature.

The measured emission spectra of a Hg(Ar) UV light source (LOT-Oriel pen-ray LSP034) were used to determine the spectral resolution of the system (FWHM 0.47 nm). This is important (especially at low temperatures and pressures) where the spectral features have a similar or smaller width. Note that data in the literature are often spectrally under-resolved (as is also the case here and in the literature), which can lead to a significant deviation in absorption cross-sections between the reported lamp measurements and the data relevant for excitation with a narrowband laser. As an example, the peak absorption at 267 nm reported by Koban et al. [17] for room temperature and atmospheric pressure that was measured with an estimated FWHM of 1.5 nm is 20% lower than our value with the current achievable spectral resolution of FWHM = 0.47 nm of our system.

4.2 Fluorescence experiments

For each condition, 1000 individual single-shot measurements were acquired and stored. To compensate for temporal jitter, the time axis of the measured signal trace was shifted according to a jitter correction (Hamamatsu software) that adjusts the time axis to the measured initial signal rise and that is applied to each individual camera image before pulse-averaged images were formed. The software-based jitter correction has been tested by alternatively coupling a small fraction of the laser beam into the spectrometer via an optical fiber that bypasses the experiment. Using the laser peak as reference for the jitter correction gave the same results as the software-based jitter correction that adjusts the time axis to the measured initial rise in LIF signal.

A background image was subtracted that was obtained with the streak camera, while the laser was firing with pure N₂ flowing through the cell. Resulting sample images for both tracers are shown in Fig. 3 with calibrated wavelength and time axis. These images deliver wavelength-specific temporal profiles (horizontal binning of columns) and fluorescence spectra for specific time intervals (vertical binning of rows) after laser excitation. It was found that, within the error limits (variation below 5%), the number of binned columns did not influence the evaluated effective fluorescence lifetimes, i.e., there was no measurable dependence of the fluorescence lifetime on the emission wavelength. Therefore, the signal-to-noise ratio was enhanced by averaging pixel counts within columns covering the spectral range between 265 and 350 nm for XL and between 270 and 360 nm for TMB. Fluorescence spectra were determined by binning a number of rows in the range of significant pixel counts. The resulting spectra were corrected for the instrument spectral response by recording emission spectra of a deuterium lamp with known spectral radiance using the same optical setup. While the recorded tracer fluorescence showed a gradual variation in intensities and red-shift with increasing temperature, above certain (species and bath-gas specific) temperatures, dramatic changes occurred both in intensity and emission spectra. These were attributed to tracer decomposition and oxidation as reported before [5, 15] and investigated in more detail for toluene in specific high-temperature experiments in shock tubes [25].

Figure 4 presents examples of LIF excitation/decay profiles for each species for three temperatures. Because the fluorescence decay times strongly vary depending on the environmental conditions, the sweep time of the streak tube needs to be adjusted to detect the entire signal trace on the full height of the CCD, which also influences the resulting time resolution of the setup. The temporal instrument

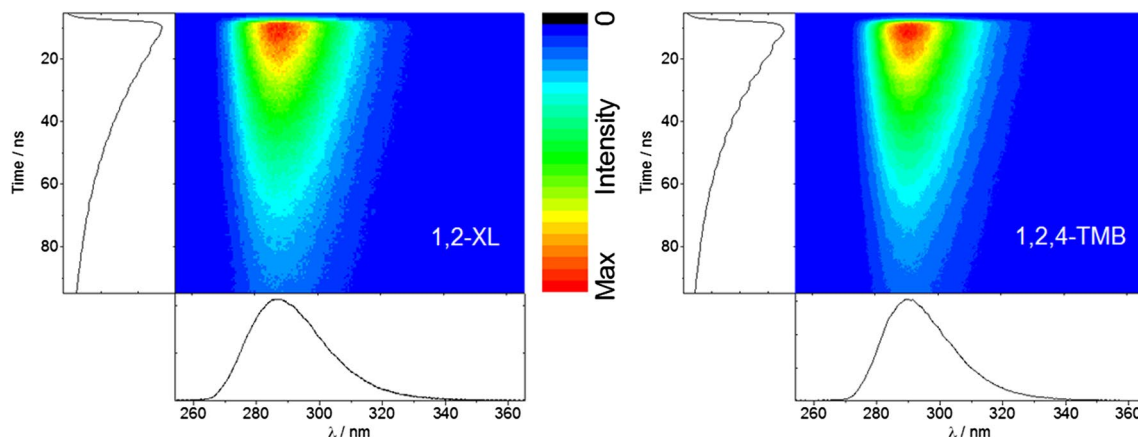


Fig. 3 Spectrally and temporally resolved fluorescence (color coded) after excitation at 266 nm of XL (left) and TMB (right). Conditions: Temperature: 296 K, 2 mbar XL or TMB in N₂, total pressure: 1 bar.

Solid lines: signal integration along the time axis results in the plotted spectral profiles (bottom: spectra) and along the spectral axis the decay profiles (left: fluorescence-intensity-time traces)

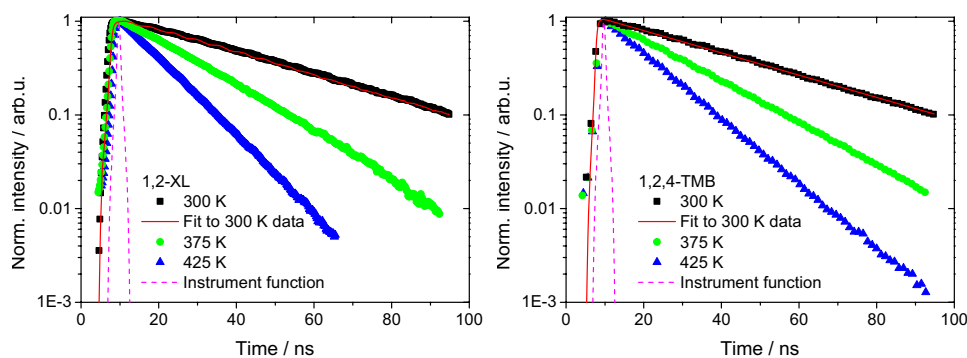


Fig. 4 Time-resolved measurements of the fluorescence intensity for XL (left) and TMB (right) in 1 bar N_2 with excitation at 266 nm at various temperatures. For 300 K, the fitted convolution functions are

function is measured using the stray light from the picosecond laser pulse in the absence of tracers and shown in Fig. 4. For the fastest decays, the minimum temporal resolution of the detection system is 25 ps FWHM.

Signal decay times τ were determined using the convolve-and-compare method [26]. A convolution of a single- or double-exponential decay with the measured instrument response function was least-squares fitted to the experimental excitation/decay profiles. Figure 4 shows examples of this fitting procedure for each species using mono-exponential decay functions (red lines) for the room-temperature data (black dots). Fitting parameters are the decay time, the signal amplitude, and a temporal shift to optimize the instance where experimental and simulated signal intensities reach their respective peak values.

5 Results

5.1 Absorption cross-section

To verify that the absorption experiments provide reliable data, spectra of TL were recorded as a well-documented reference case, and are presented for a range of temperatures in Fig. 5 (upper left). Our own measurements (solid lines) are compared to data from Koban et al. [17] at three temperatures (dashed lines). Our new data are in close agreement with the earlier results. The upper right and the lower left panel in Fig. 5 show the absorption cross-sections of XL and TMB for a range of temperatures. All the spectra show a characteristic band structure that is most prominent at low temperatures but can be recognized almost up to the highest temperatures investigated. Although the spectral resolution of the lamp measurement is quite good ($0.47 \text{ nm FWHM} \approx 75 \text{ cm}^{-1}$ at 250 nm), cf. arrows in Fig. 5 as determined by the FWHM of a recorded mercury line at 254 nm from a low-pressure discharge lamp, the spectra are still

shown as red lines. The instrument response (dashed magenta lines) was recorded from laser stray light for the same streak settings chosen for the measurements at the respective lowest temperature

under-resolved at low temperatures compared to highly resolved spectra of Etzkorn et al. (resolution $\approx 23 \text{ cm}^{-1}$) [27] and Fally et al. (resolution $\approx 1 \text{ cm}^{-1}$) [28]. It is apparent from Fig. 5 that the much better resolution of the narrow vibrational and rotational structure can lead to up to 80% higher peak values.

The absorption spectra of XL and TMB red-shift with increasing temperature and the cross-sections increase slightly, as it is the case for TL. At the same time, the spectra of all species broaden towards the long-wavelength side. With increasing temperature, a strong band below 230 nm emerges that represents $S_0 \rightarrow S_2$ transitions that become accessible due to increasing thermal population of higher vibrational states in the S_0 level. The lower right panel shows the data from the lamp measurements at 266 nm (solid symbols) compared to laser-based absorption measurements (open symbols) [14, 17] together with respective fit functions (function in the first row in Table 2 and parameters in Table 3). The fit functions for TL and TMB were generated with the laser-based results, since their temperature exceeded those measured with the lamp. The reduced values of the lamp data towards lower temperatures (below $\sim 400 \text{ K}$ in case of TMB) are a result of the insufficient spectral resolution close to the spectral peak near 266 nm. However, the small deviation shows that the spectral resolution in our measurements is high enough to cause a $< 20\%$ deviation even at room temperature.

5.2 Fluorescence spectra

Fluorescence spectra of TL [15], XL, and TMB are shown in Fig. 6 for a series of temperatures in 1 bar N_2 , normalized to their respective peak intensities. To reduce noise, the spectra were smoothed by an adjacent-average filter with a window size of 2 nm.

As expected, for temperatures up to 875 K, the overall spectral signatures of the three methyl-substituted

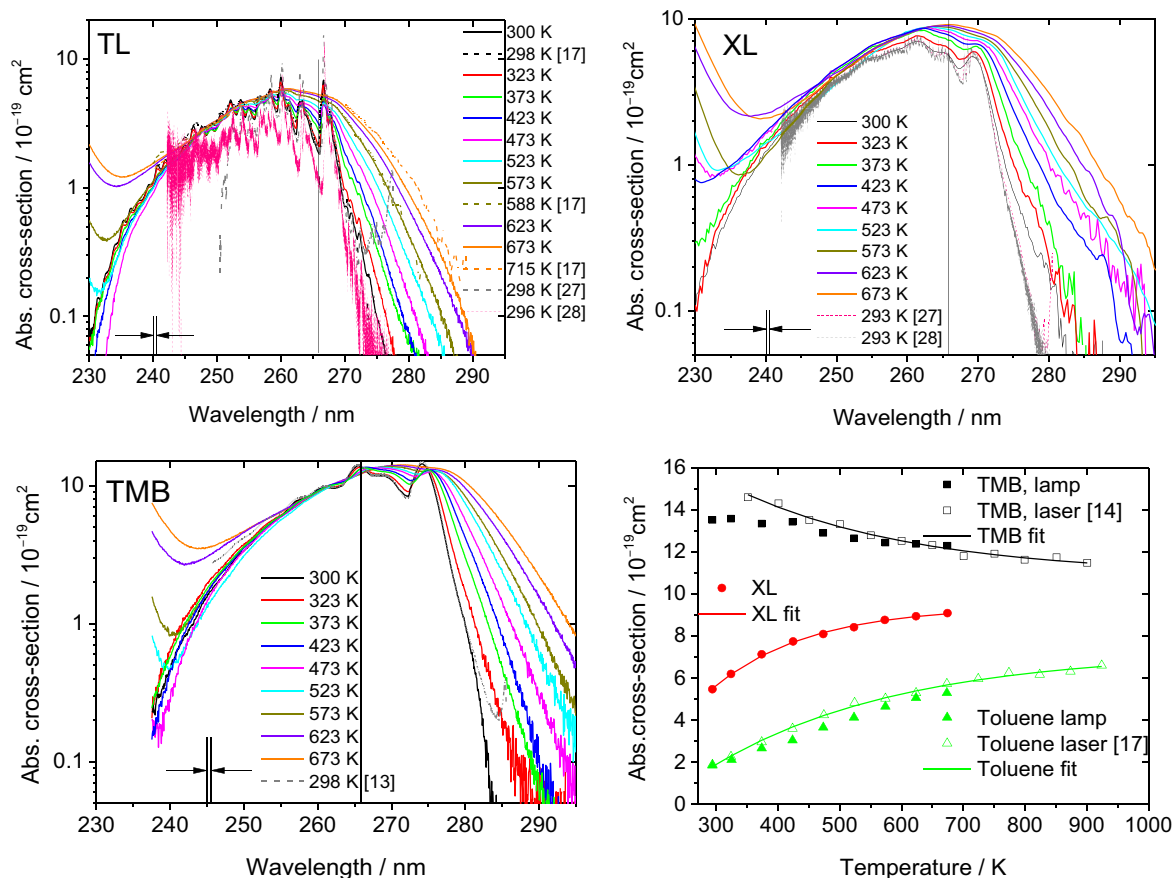


Fig. 5 Absorption spectra of TL (upper left), XL (upper right), and TMB (lower left) at various temperatures in 1 bar N₂. The arrows indicate the spectral resolution (0.47 nm FWHM). Results from Koban et al. [17], Etzkorn et al. [27], and Fally et al. [28] are plotted for comparison. Lower right: absorption cross-sections at 266 nm determined from the spectra (solid symbols) and the laser meas-

urements (open symbols) with fits based on the function given in Table 2. Literature data from Koban et al. [17] and Rossow [14]. While the fluctuations and deviation from the references for low absorption cross-sections represent noise, the structure reported at room temperature in the data from Etzkorn et al. [27] and Fally et al. [28] is considered real and originates from vibrational structure

Table 2 Factors represented in the model function (Eq. 6) for deriving relative fluorescence signal strengths of TL, XL, and TMB

Absorption cross-section	$\sigma(T) = \sigma_0 + \sigma_1 \exp\left(-\frac{T}{\sigma_2}\right)$
Fluorescence lifetime of the ATEL	$\tau(T) = \tau_0 + \tau_1 \exp\left(-\frac{T}{\tau_2}\right) + \tau_3 \exp\left(-\frac{T}{\tau_4}\right)$
Quenching coefficient	$q(T) = q_0 + q_1 \exp\left(-\frac{T}{q_2}\right)$
Total pressure correction	$c(T, p_{\text{tot}}, p_{\text{O}_2}) = \frac{c_0}{1 + c_{12} \exp(-c_2 p_{\text{O}_2})} \exp\left(-\frac{(c_3 - T)^2}{c_4}\right) \times \exp\left(-\frac{(p_{\text{tot}} - 1)c_5}{1 + c_{12} \exp(-c_2 p_{\text{O}_2})}\right) + 0.87$

Pressure is in bar and temperature in K

single-ring aromatics are quite similar with respect to peak position and half width. At room temperature, the spectra of XL and TMB peak at 287 and 290 nm (FWHM: 28 and 25 nm, respectively). In agreement with Nijegorodov et al. [29], these positions are red-shifted compared to toluene (280 nm) having a single methyl group. The result for TMB is in rough accordance with the data

from Rossow [14], where at 350 K, a peak position of 285 nm and a FWHM of 30 nm were determined. With increasing temperature (up to 875 K), a slight red-shift of about 2.3 nm/100 K for XL and 2.5 nm/100 K for TMB is observed, the latter being slightly lower than that measured by Rossow [14] who reported 3.6 ± 0.6 nm/100 K. Toluene shows a lower red-shift of 2.0 nm/100 K [30]. In

Table 3 List of parameters used in the functional forms comprising the model function (Eq. 6) for TL, XL, and TMB

	TL	XL	TMB
σ_0	7.2537×10^{-19}	9.4226×10^{-19}	1.0903×10^{-18}
σ_1	-1.4249×10^{-18}	-2.4575×10^{-18}	1.2742×10^{-18}
σ_2	305.9	159.13	290.98
τ_0	4×10^{-11}	–	–
τ_1	1.4085×10^{-5}	5.4939×10^{-6}	2.4723×10^{-6}
τ_2	51.48	61.777	72.111
τ_3	–	1.5447×10^{-9}	1.2047×10^{-8}
τ_4	–	301.73	180.85
q_0	0.1	0	0.92254
q_1	93,306	43,341	21,072
q_2	51.48	61.777	71.458
c_0	13.96	3.1974	0.97566
c_1	11.66	8.4352	11,318
c_2	2.87	5.8824	0.006913
c_3	642.25	628.92	512.39
c_4	27,576	33,067	19,257
c_5	0.19	0.56184	0.46988
k_f	5.90×10^6	8.19×10^6	1.22×10^7

k_f is the fluorescence rate constant derived from [29]

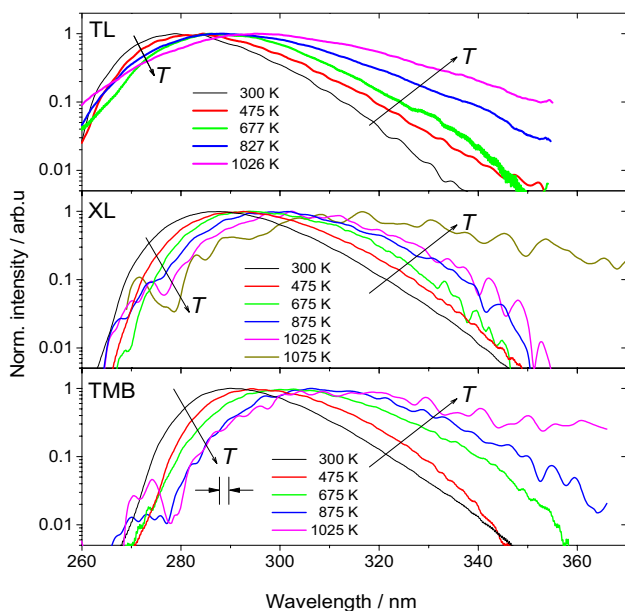


Fig. 6 Peak-normalized fluorescence spectra of TL [15], XL, and TMB at various temperatures in 1 bar N_2 after excitation at 266 nm. The signal-to-noise ratios get low at higher temperatures, resulting in a wavy structure. Number densities of XL and TMB were kept constant at $\sim 2 \times 10^{23} \text{ m}^{-3}$ independent of the temperature. The arrows show the spectral resolution of the detection system derived from measurements with a Hg lamp. The arrows indicate the trends with increasing temperature

the same temperature range, the half widths increase by approx. 12 and 29%, respectively.

For higher temperatures, a much larger apparent shift is observed. This is attributed to the onset of pyrolysis as studied in more detail for species like anisole in shock tubes [25]. Because of this effect, the temperature-dependent measurements presented in this work end at 1075 K. Below, the respective tracers are considered stable on the time scale of the experiment. In the present experiments, a possible fine structure of the spectra observed at lower temperature is smeared out due to the limited spectral resolution of about 1.9 nm (indicated by the arrows in Fig. 6).

In the presence of O_2 , the fluorescence spectra red-shift additionally (Fig. 7), which are mostly linear with the O_2 partial pressure. The red-shift from pure nitrogen to air (210 mbar at 1 bar total pressure) is roughly equivalent to a temperature increase of 100 K. This effect is stable (within the error limits) for the investigated temperature range.

All data for the center wavelength of the fluorescence spectra for XL and TMB and even an old data set of TL are presented in Fig. 8. The centre wavelength was determined by the mean value of the FWHM-border positions. This was the preferred method over, e.g., the integral mean value, because all red-shift values and trends were the same, but the results show reduced scatter.

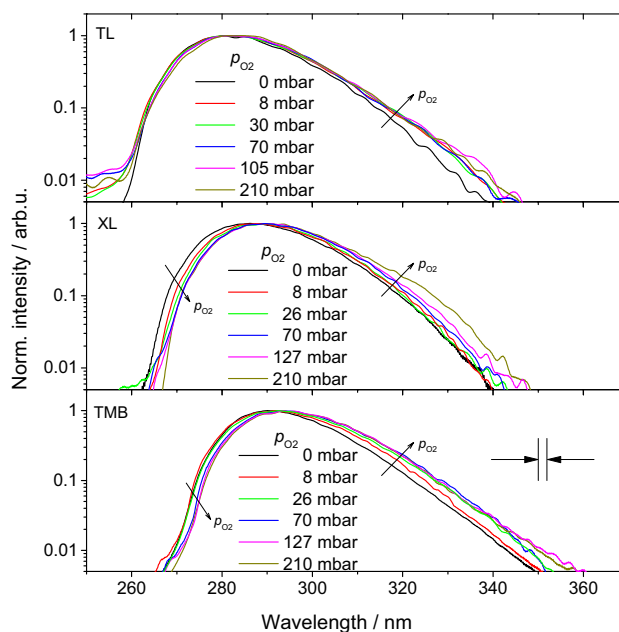


Fig. 7 Peak-normalized fluorescence spectra of TL, XL, and TMB at various O_2 partial pressures, 1 bar total pressure at room temperature (296 K) after excitation at 266 nm. Number densities of TL, XL, and TMB were kept constant at $\sim 2 \times 10^{23} \text{ m}^{-3}$ independent of the bath-gas composition. The arrows show the spectral resolution of the detection system derived from measurements with a Hg lamp. The arrows indicate the trends with increasing O_2 partial pressure

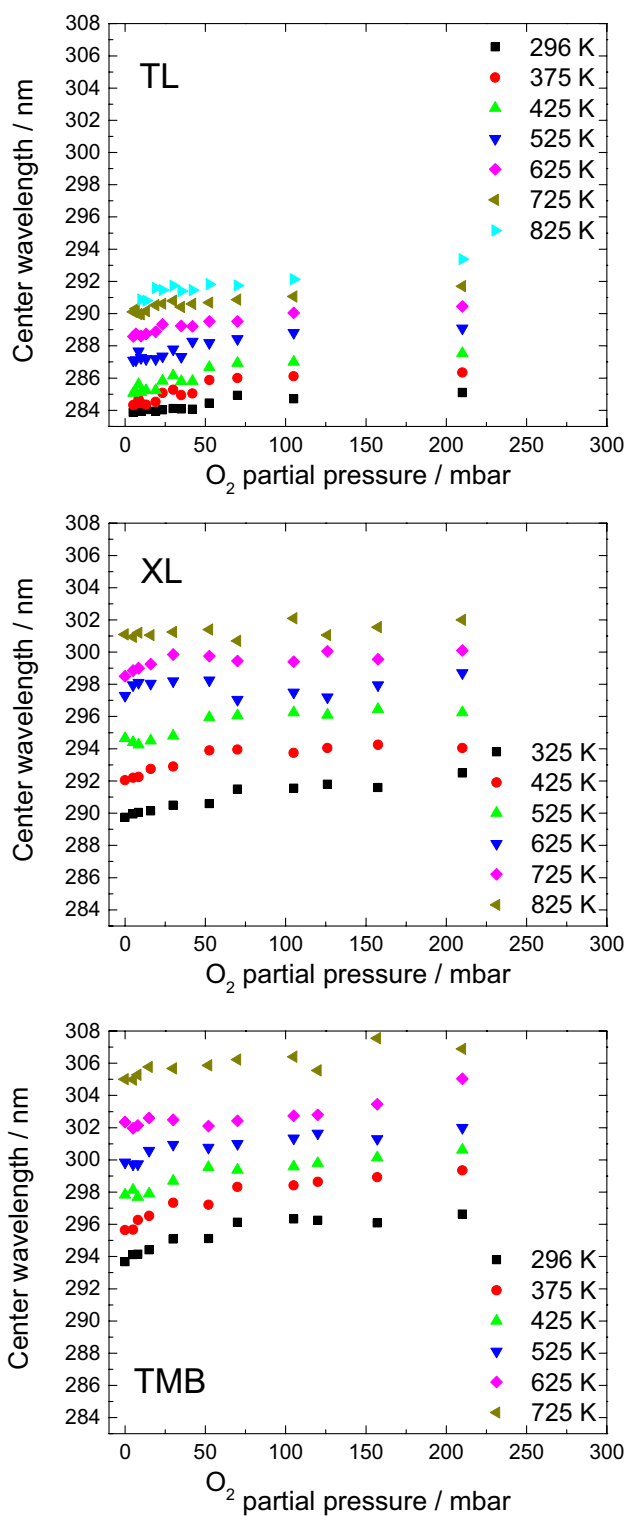


Fig. 8 Temperature- and O₂ partial-pressure-dependent center wavelength (determined from the average FWHM positions). The wavelength as well as the temperature-dependent red-shift increases from TL (upper left panel) over XL (upper right panel) to TMB (lower left panel)

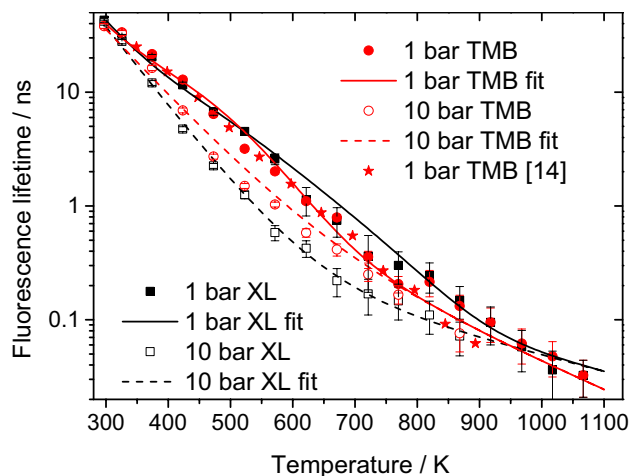


Fig. 9 Effective fluorescence lifetimes of XL and TMB in N₂ as a function of temperature for 1 and 10 bar. FQY data from Rossow [14] (red stars) are normalized to lifetimes at 350 K. Solid lines are taken from the model introduced in Sect. 5.3

5.3 Effective fluorescence lifetimes

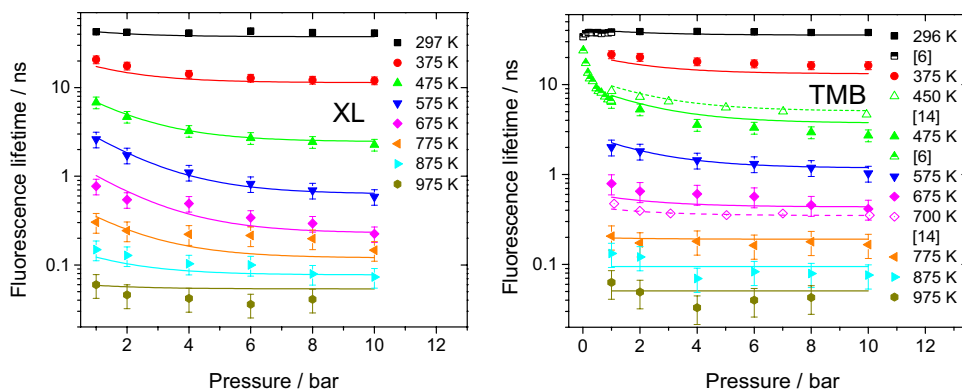
5.3.1 Nitrogen bath gas

Following the procedure outlined in Sect. 4.2, effective fluorescence lifetimes of XL and TMB diluted in N₂ were determined (Fig. 9). All error bars in the upcoming sections were determined from the standard deviation of multiple measurements or in case of single measurements, the uncertainties of the fitting procedure presented in Sect. 4.2 were used for estimating errors. In the explored temperature range, the fluorescence lifetimes of XL and TMB decrease by three orders of magnitude, whereby the decrease is slightly stronger at higher pressures. The dependence can be approximated reasonably well by $c(T, p_{\text{tot}}, p_{\text{O}_2}) \tau(T)$ presented in Table 2.

Our temperature-dependent fluorescence lifetimes for TMB at 1 bar obtained from time-resolved measurements (solid red circles Fig. 9) correlate well with the data calculated from relative FQYs from Rossow [14] that were determined from spectrally integrated fluorescence intensities measured at 350–900 K and normalized to the lifetime value at 350 K (red stars).

Figure 10 shows that the fluorescence lifetimes slightly decrease with increasing pressure. The overall trend with pressure and temperature is similar for XL and TMB. The room-temperature data of TMB are an exception showing a slight increase of the fluorescence lifetime with pressure. The effect of increasing fluorescence lifetime, the so-called photo-induced cooling effect, was first theoretically described by Wadi et al. [31] and experimentally tested for

Fig. 10 Pressure dependence of the effective fluorescence lifetimes of XL (left) and TMB (right) for a range of temperatures with additional data from [13] (data from 0 to 1 bar) and [14] (hollow symbols and dashed lines). The solid lines are simulations based on the model introduced in Sect. 5.3



naphthalene by He et al. [32], while the more stabilizing effect of increased pressure was first described theoretically and experimentally proven for naphthalene by Beddard et al. [33]. This photo-induced cooling effect for TMB was experimentally shown and explained by us before for studies at sub-atmospheric pressures [13], where we discussed the importance of collision-induced vibrational relaxation in excited aromatic molecules by reducing the total pressure and, therefore, the collision frequency. The higher pressure data points from this study smoothly continue the previously described trend (Fig. 10).

The decrease in fluorescence lifetimes with increasing pressure is stronger at moderate temperatures and flattens out at higher temperatures, most probably due to the fact that the fluorescence lifetimes become too short for the pressure-induced increase in collision frequency to show an effect. A similar quenching effect with N_2 was also observed by Rossow [14] for the spectrally integrated TMB fluorescence intensities at 450 and 700 K, where a decrease in signal intensity was observed by about a factor of 1.9 and 1.3, respectively, when increasing the buffer gas pressure from 1 to 10 bar. This effect is weaker compared to that observed for toluene where the decrease was by a factor of 3 and 2.5 for 450 and 700 K, respectively. When normalizing the data

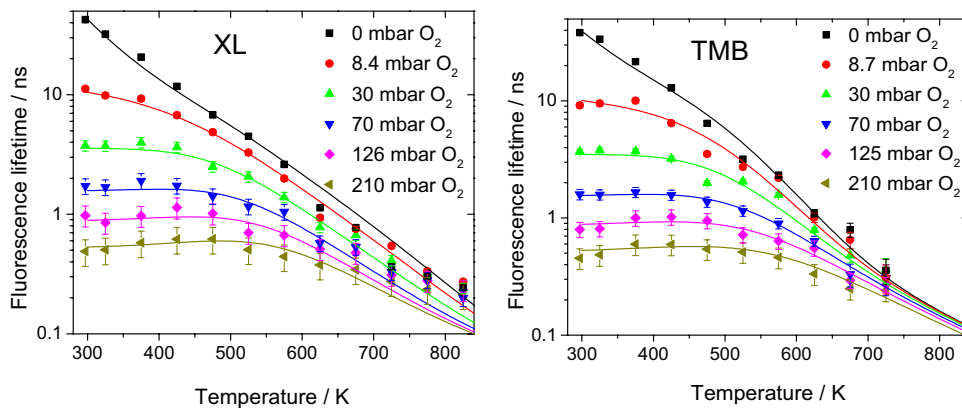
from Rossow [14] with the respective lifetimes at 1 bar of the fluorescence model introduced in Sect. 5.3, the trends of both data sets show good agreement (Fig. 10, right).

5.3.2 N_2/O_2 mixtures as bath gas

Figure 11 shows fluorescence lifetimes of XL and TMB in atmospheric pressure N_2/O_2 mixtures with various partial pressures of O_2 as a function of temperature. As the comparison in both graphs shows for the case of pure N_2 (filled black squares), quenching by O_2 is most efficient at lower temperatures and is almost independent of the O_2 partial pressure at the highest temperatures investigated. At room temperature, when a mixture equal to dry air at 1 bar is used, the fluorescence lifetime of XL and TMB decreases by a factor of 84 and 89, respectively, with respect to the values in pure N_2 . This behavior is similar to that reported for TL [15]. Except for the lowest O_2 partial pressures, the measured lifetimes exhibit a shallow maximum as a function of temperature which is shifted to higher temperatures with increasing O_2 partial pressures.

It was shown in the previous work that the quenching efficiency of toluene shows Stern–Volmer behavior. This was deduced either from spectrally and temporally integrated

Fig. 11 Effective fluorescence lifetimes of XL (left) and TMB (right) as a function of temperature for various O_2 partial pressures in N_2 at a total pressure of 1 bar. Solid lines are simulations based on the model introduced in Sect. 5.4



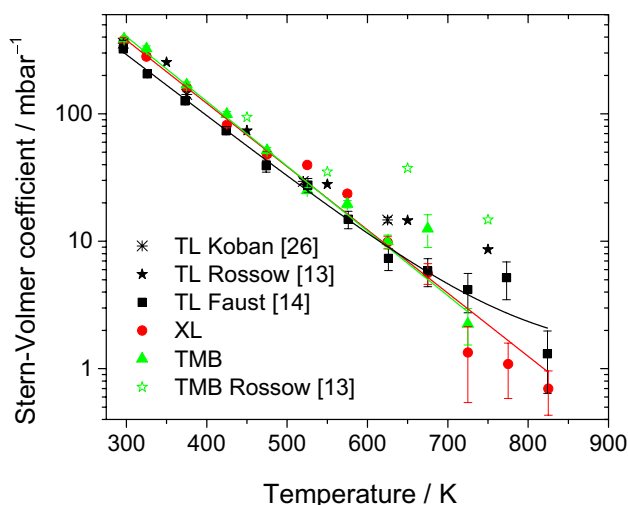


Fig. 12 Stern–Volmer coefficients for O₂ quenching of TL, XL, and TMB as a function of temperature. Lines are mono-exponential fits to the TL data of Faust et al. [15, 21] and our present data

fluorescence intensities [14, 20] or from fluorescence lifetime measurements [15]. In the present work, Stern–Volmer coefficients for XL and TMB were determined according to Eq. (3) for various temperatures from the slopes of the fluorescence lifetime data vs. inverse O₂ partial pressure. The resulting temperature-dependent Stern–Volmer coefficients for quenching of XL and TMB by O₂ are shown in Fig. 12 together with values from Koban et al. [17], Faust et al. [15], and Rossow for TL [14], as well as from Rossow for TMB [14]. There is overall agreement for TMB for the lower temperatures, but the deviations between Rossow and our data become significant at higher temperatures. This could be due to the different measurement techniques (our more direct fluorescence lifetime method vs. the fluorescence-intensity method) and can (to some extent) also be seen in the toluene data. However, there is almost the same trend with temperature in our data for XL and TMB which is further emphasized by the extended data for TL from Faust et al. [21] which also takes high-pressure data in air (up to 10 bar) into account.

5.4 Model functions

In the following, a semi-empirical model—based on the work by Koban et al. [17]—is introduced for predicting the temperature, total pressure, and O₂ partial-pressure dependence of the relative fluorescence quantum yield, ϕ_{fl} , of the methyl-substituted single-ring aromatics investigated in this work. One simplification made in Koban’s fluorescence model for TL [17] was the neglect of the effect of total pressure on ϕ_{fl} . That model was extended by Faust et al. [21] to take total pressure into account:

$$\phi_{fl}(T, n_{O_2}) = \left[\frac{A_1(\lambda_{exc}, T)}{1 + k_{SV,1} n_{O_2}} + \frac{A_2(\lambda_{exc}, T)}{1 + k_{SV,2} n_{O_2}} \right] \left[B_1(T) \exp\left(-\frac{P_{tot}}{B_2(T)}\right) + B_3(T) \right]. \tag{5}$$

In this equation, the first term considers the temperature and O₂-quenching dependent ϕ_{fl} originating from Koban et al., while the second term describes the dependence on the total pressure.

Both models, however, cannot predict the fluorescence signal in air above atmospheric pressure. This is due to the fact that $k_{SV,2}$ is given as a linear function of temperature, which will give negative values for $k_{SV,2}$ above 720 K, resulting in non-physical behavior and a strong failure in predicting measured fluorescence intensities for TL for high number densities of O₂ (blue dotted lines in left panel in Fig. 13). Therefore, we will present a new model for TL in this section, which is able to predict the fluorescence signal per molecule even for high pressures in air for a large range of environmental conditions. The signal intensity per molecule for 266 nm excitation for all three tracer species can then be calculated from:

$$S \sim \sigma(266 \text{ nm}, T) \phi(266 \text{ nm}, T, p_{tot}, p_{O_2}) = \sigma(T) \frac{k_f c(T, p_{tot}, p_{O_2}) \tau(T)}{1 + q(T) p_{O_2}}. \tag{6}$$

This equation is basically identical to Eq. (3) multiplied by the absorption cross-section (just like in the Koban model) and predicts the absorption cross-section times the fluorescence quantum yield for 266 nm and is, therefore, proportional to the signal intensity per molecule. Therefore,

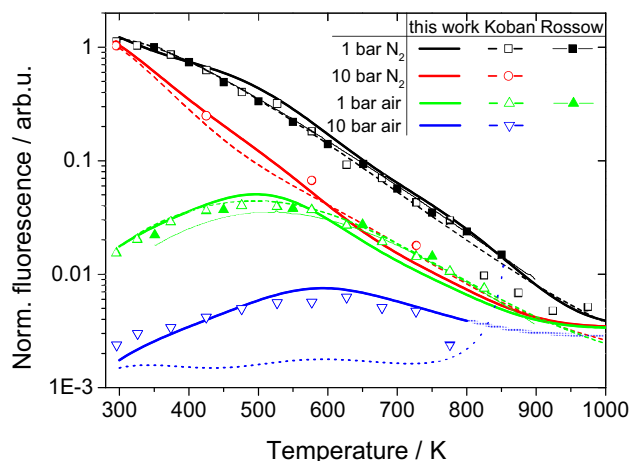


Fig. 13 Comparing the extended Koban model (dashed lines) [21] and the photo-physical model of Rossow (solid lines) [14] for toluene with our new model (heavy lines). Respective measurements from Koban and Faust (open symbols) [15, 21] and from Rossow (solid symbols) [14]

multiplying Eq. (6) with the number density and the total pressure yields the LIF signal intensity per volume. The difference to the Koban model is that now there is just one quenching coefficient $q(T)$, which prevents singularities with the downside that it is not the Stern–Volmer coefficient. $\tau(T)$ represents the fluorescence lifetime of the average thermal energy level (ATEL) in S_1 , while $c(T, p_{\text{tot}}, p_{\text{O}_2})$ is a correction factor taking into account the energy difference between the initially excited energy level and the ATEL of S_1 and the following collisional cascade. This was inspired by the step-ladder model of Thurber [34] and Koch [35]. The correction factor depends on the fluorescence lifetime which is why it also depends on temperature, total pressure, and O_2 partial pressure. This model can (with different parameters), as well, predict the fluorescence signal of XL and TMB. All model parameters were determined by globally fitting Eq. (6) to all the toluene data of Faust et al. [15, 21] and the experimental data for XL and TMB presented in Sect. 5.2.

Table 2 presents a collection of the different factors forming the model function (Eq. 6), while Table 3 lists all relevant fit parameters.

Figure 13 compares the new toluene model to the older ones. As one can see, it predicts the fluorescence intensity for high-pressure high-temperature conditions in air better than the old ones. Because there are no data for high pressure in air for temperatures above 800 K, at higher temperatures, we cannot assess the correctness of the data extrapolated based on the model (light blue line).

Figure 14 compares the expected fluorescence signal (derived from fluorescence lifetimes) per molecule for TL, XL, and TMB in the temperature range from 300 to 1000 K for N_2 and air at 1 and 10 bar total pressure, respectively. Overall, the signal of TMB is the strongest among these three tracers, apart from temperatures above 800 K and high

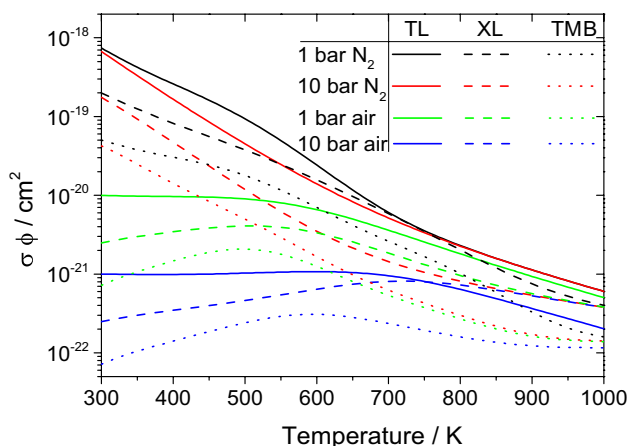


Fig. 14 Fluorescence signal per molecule in air and N_2 for 1 and 10 bar predicted from Eq. (6) for TL (dotted lines), XL (dashed lines), and TMB (solid lines)

O_2 partial pressures, where the signal of XL exceeds the one of TMB. The signal of TL is overall the weakest of the methylbenzenes, at least on a per-molecule basis.

The model was created and derived from fluorescence lifetime data presented in previous and the current work for temperatures from 296 to 1000 K without O_2 , and up to 800 K in the presence of O_2 for total pressures up to 10 bar air. Due to the choice of the implemented fit functions, no non-physical behavior (e.g., singularities) is expected for higher temperatures, pressures, or O_2 partial pressures.

Comparisons between the model and the experimental data are shown in Fig. 9 (temperature dependence), Fig. 10 (total pressure dependence), and Fig. 11 (O_2 partial-pressure dependence). As one can see, the model is capable to describe all experimental results (in the given error estimation). In case of XL and TMB, the overall agreement with the experimental data is very good. The mean relative errors of the model are 12.6, 13.2, and 11.1% for TL, XL, and TMB, respectively, calculated by averaging the relative model error of all available data points. Thus, the model describes all three species similarly well.

6 Discussion

The presented absorption spectra of toluene, *o*-xylene, and 1,2,4-trimethylbenzene (Fig. 5) are in good agreement with the literature data for room temperature from Koban [17], Etkorn [27], and Fally [28], while the retrieved absorption cross-sections at 266 nm follow the trend of temperature-dependent laser absorption measurements of Koban [17] and Rossow [14]. There are deviations ($\sim 10\%$) for TMB between the laser absorption measurements from Rossow and our deuterium lamp data in the region below 450 K that are attributed to slightly under-resolving the spectral features at these temperatures. The trends of the absorption cross-section retrieved at 266 nm shown in Fig. 5 can be explained from the general variation of the spectra with temperature: All three absorption spectra red-shift, broaden, and increase in cross-section with temperature due to the spread in thermal population towards higher vibrational levels. The laser absorption data of TL and TMB were used to create fit functions for the absorption cross-section for these species at 266 nm, since they cover a broader temperature range and are also considered more reliable at low temperatures where the spectrometer measurements tend to provide under-resolved data. The maximum deviation of our data at 266 nm from literature values is 15% at room temperature and the deviation diminishes at higher temperatures.

The increase or decrease in the fluorescence lifetime of various tracers with increasing pressure in the sub-atmospheric pressure regime upon 266 nm excitation was discussed in detail in a previous publication [13], although in

this case, apart from TMB at room temperature, the fluorescence lifetime always decreases with increasing pressure.

The effect of the so-called “third decay channel” [36] that describes the occurrence of an additional fast decay channel above a limiting temperature also applies to XL and TMB. Above 525 K for XL and 475 K for TMB, an additional, short lifetime component (τ in the range of < 1 ns) can be observed in the fluorescence decay. However, we focused on the long lifetime component in this study, thus using only the longer decay constant from double-exponential fitting the fluorescence decay as explained in Sect. 4.2.

The Stern–Volmer coefficients for TMB are in good agreement with values from Rossow [14] for low temperatures, but show increasingly larger deviation with increasing temperature. However, the data pool in [14] just consists of four points of which one was neglected for further analysis (the value at 650 K of Rossow in Fig. 12). Our Stern–Volmer coefficients of XL and TMB show consistent trends and also correspond well with the extended data of Faust et al. [21]. We therefore prefer the new data over the data reported in [14]. However, since it enabled to improve the quality of the fit, the quenching constant in the model was allowed to deviate from the Stern–Volmer coefficients, thus trading the quality of the fit over the strict physical meaning of the fit constants.

Overall, the discussed methylbenzene derivatives exhibit similar photo-physical properties and thus are similarly applicable for LIF imaging measurements. For practical considerations; however, there are some important differences. The signal per molecule increases with each additional methyl group because of the increasing absorption cross-sections. In LIF experiments, however, the effective signal is sometimes limited by the vapor pressure of the tracer which is lower for the heavier species. In combination, the maximum achievable signal is comparable for all three species. TMB is advantageous if a strong signal per molecule is desired (one order of magnitude stronger signal-per-molecule compared to toluene). TMB also has advantages in the context of two-color thermometry, because its temperature-induced fluorescence red-shift is more pronounced compared to toluene, resulting in an enhanced temperature sensitivity. In terms of quenching by O_2 , the spectra are also shifted to the red by roughly the same amount as a 100 K temperature increase for a 210 mbar O_2 partial pressure rise. This effect is stable for all three molecules as well as all temperatures investigated in this study.

7 Conclusions

The spectroscopic properties of the three structurally similar gas-phase fluorescence tracers with different vapor pressures toluene (TL), *o*-xylene (XL), and 1,2,4-trimethylbenzene

(TMB) were investigated in terms of absorption spectra, fluorescence spectra, and effective fluorescence lifetimes. Measurements were conducted as a function of temperature, bath-gas pressure, and oxygen partial pressure in parameter ranges typical for tracer LIF diagnostics in practical applications. Spectrally and temporally resolved fluorescence measurements were obtained upon picosecond laser excitation with a streak camera coupled to a spectrometer. There is a spectral red-shift of the fluorescence peak with temperature of 2.3 and 2.5 nm/100 K for XL and TMB, respectively, as well as a spectral red-shift by oxygen of ~ 2 nm/100 mbar O_2 for both species. With increasing temperature, the fluorescence lifetime decreases significantly by a factor of ~ 3 ns/100 K in a similar fashion for both, XL and TMB. Higher total pressures enhance this decrease for both species. As for TL, O_2 is a strong fluorescence quencher for XL and TMB, and the Stern–Volmer factors derived for XL and TMB are larger than those of TL at room temperature. At 725 K range, O_2 quenching is reduced by roughly a factor of 200 for XL and TMB compared to room temperature, making them significantly less affected by oxygen quenching compared to TL at elevated temperatures.

A new semi-empirical model similar to the one of Koban et al. [17] is introduced for all three species. The measured absorption cross-sections and effective fluorescence lifetimes of toluene [15, 21] were used to validate the model and the model was compared to the one of Koban et al. [17] and Rossow [14]. The new model has the benefit of being able to predict signals at higher pressures in the presence of O_2 compared to the previous ones that were limited to peak partial pressures of 0.21 bar O_2 . The same model was used to predict relative LIF signal intensities for TL, XL, and TMB using a specific set of parameters for each species. All these parameters were determined through a global fitting routine to minimize the overall errors in the model. In the range of conditions where this model was validated (i.e., 300–1000 K, up to 10 bar in pure N_2 and at 1 bar for environments between pure N_2 and air composition), we found good agreement between the modelled and the measured fluorescence lifetimes as well as literature data.

Acknowledgements The authors acknowledge funding by the Deutsche Forschungsgemeinschaft (SCHU 1369/28) and the FVV (Forschungsvereinigung Verbrennungskraftmaschinen) Bioptic III project, FVV-Nr. 9000010.

References

1. C. Schulz, V. Sick, Prog. Energy Combust. Sci. **31**, 75 (2005)
2. B. Peterson, D.L. Reuss, V. Sick, Proc. Combust. Inst. **33**, 3089 (2011)
3. M. Loeffler, F. Beyrau, A. Leipertz, Appl. Opt. **49**, 37 (2010)

4. S. Lind, S. Abmann, L. Zigan, S. Will, *Appl. Opt.* **55**, 1551 (2016)
5. S. Faust, T. Dreier, C. Schulz, *Appl. Phys. B* **112**, 203 (2013)
6. T. Benzler, T. Dreier, C. Schulz, *Appl. Phys. B* **123**, 39 (2017)
7. S. Faust, M. Goschütz, S.A. Kaiser, T. Dreier, C. Schulz, *Appl. Phys. B* **117**, 183 (2014)
8. L.M. Itani, G. Bruneaux, A.Di Lella, C. Schulz, *Proc. Combust. Inst.* **35**, 2915 (2015)
9. J. Trost, L. Zigan, A. Leipertz, D. Sahoo, P.C. Miles, *Appl. Opt.* **52**, 8001 (2013)
10. C. Schulz, J. Gronki, S. Andersson, SAE technical paper series 2004-01-1917 (2004)
11. D. Frieden, V. Sick, J. Gronki, C. Schulz, *Appl. Phys. B* **75**, 137 (2002)
12. A. Bolovinos, J. Philis, E. Pantos, P. Tsekeris, G. Andritsopoulos, *J. Mol. Spectrosc.* **94**, 55 (1982)
13. T. Benzler, S. Faust, T. Dreier, C. Schulz, *Appl. Phys. B* **121**, 549 (2015)
14. B. Rossow, *Photophysical Processes of Organic Fluorescent Molecules and Kerosene—Application to Combustion Engines* (Université Paris-Sud 11, Paris, 2011)
15. S. Faust, T. Dreier, C. Schulz, *Chem. Phys.* **383**, 6 (2011)
16. F. Ossler, T. Metz, M. Aldén, *Appl. Phys. B* **72**, 465 (2001)
17. W. Koban, J.D. Koch, R.K. Hanson, C. Schulz, *Phys. Chem. Chem. Phys.* **6**, 2940 (2004)
18. J.R. Lakowicz, *Principles of Fluorescence Spectroscopy* (Springer Science + Business Media, LLC, New York, 2006)
19. S.A. Kaiser, M.B. Long, *Proc. Combust. Inst.* **30**, 1555 (2005)
20. W. Koban, J.D. Koch, R.K. Hanson, C. Schulz, *Appl. Phys. B* **80**, 777 (2005)
21. S. Faust, G. Tea, T. Dreier, C. Schulz, *Appl. Phys. B* **110**, 81 (2013)
22. W. Koban, J. Schorr, C. Schulz, *Appl. Phys. B* **74**, 111 (2002)
23. R. Devillers, G. Bruneaux, C. Schulz, *Appl. Phys. B* **96**, 735 (2009)
24. D. Fuhrmann, T. Benzler, T. Fernando, T. Endres, S.A. Kaiser, T. Dreier, C. Schulz: *Proc. Combust. Inst.* **36**, 4505 (2017)
25. S. Zabeti, A. Drakon, S. Faust, T. Dreier, O. Welz, M. Fikri, C. Schulz, *Appl. Phys. B* **118**, 295 (2015)
26. T.B. Settersten, A. Dreizler, R.L. Farrow, *J. Chem. Phys.* **117**, 3173 (2002)
27. T. Eitzkorn, B. Klotz, S. Sörensen, I.V. Patroescu, I. Barnes, K.H. Becker, U. Platt, *Atmos. Environ.* **33**, 525 (1999)
28. S. Fally, M. Carleer, A.C. Vandaele, *J. Quant. Spectrosc. Radiat. Transf.* **110**, 766 (2009)
29. N. Nijegorodov, R. Mabbs, D.P. Winkoun, *Acta A* **59**, 595 (2003)
30. S. Faust, *Characterisation of Organic Fuel Tracers for Laser-Based Quantitative Diagnostics of Fuel Concentration, Temperature, and Equivalence Ratio in Practical Combustion Processes* (Universität Duisburg-Essen, Duisburg, 2013)
31. H. Wadi, E. Pollak, *J. Chem. Phys.* **110**, 11890 (1999)
32. Y. He, E. Pollak, *J. Chem. Phys.* **116**, 6088 (2002)
33. G.S. Beddard, G.R. Fleming, O.L.J. Gijzeman, G. Porter, *Proc. R. Soc. Lond. A* **340**, 519, (1974)
34. M.C. Thurber, F. Grisch, B.J. Kirby, M. Votsmeier, R.K. Hanson, *Appl. Opt.* **37**, 4963 (1998)
35. J.D. Koch, R.K. Hanson, *Appl. Phys. B* **76**, 319 (2003)
36. M. Jacon, C. Lardeux, R. Lopez-Delgado, A. Tramer, *Chem. Phys. Lett.* **24**, 145 (1977)